Side-coupled cavity model for surface plasmon-polariton transmission across a groove

John S. Q. Liu[1], Justin S. White[1], Shanhui Fan[2], and Mark L. Brongersma[1],*

[1]*Geballe Laboratory for Advanced Materials, Stanford, California 94305, USA*
[2]*Ginzton Laboratory, Stanford, California 94305, USA*
**brongersma@stanford.edu*

Abstract: We demonstrate that the transmission properties of surface plasmon-polaritons (SPPs) across a rectangular groove in a metallic film can be described by an analytical model that treats the groove as a side-coupled cavity to propagating SPPs on the metal surface. The coupling efficiency to the groove is quantified by treating it as a truncated metal-dielectric-metal (MDM) waveguide. Finite-difference frequency-domain (FDFD) simulations and mode orthogonality relations are employed to derive the basic scattering coefficients that describe the interaction between the relevant modes in the system. The modeled SPP transmission and reflection intensities show excellent agreement with full-field simulations over a wide range of groove dimensions, validating this intuitive model. The model predicts the sharp transmission minima that occur whenever an incident SPP resonantly couples to the groove. We also for the first time show the importance of evanescent, reactive MDM SPP modes to the transmission behavior. SPPs that couple to this mode are resonantly enhanced upon reflection from the bottom of the groove, leading to high field intensities and sharp transmission minima across the groove. The resonant behavior exhibited by the grooves has a number of important device applications, including SPP mirrors, filters, and modulators.

OCIS codes: (240.6680) Surface plasmons

References and links

1. R. Zia, J. Schuller, A. Chandran, and M. Brongersma, "Plasmonics: the next chip-scale technology," Mater. Today **9**(7-8), 20–27 (2006).
2. H. A. Atwater, "The promise of plasmonics," Sci. Am. **296**(4), 56–63 (2007).
3. T. W. Ebbesen, C. Genet, and S. I. Bozhevolnyi,"Surface-plasmon circuitry," Phys. Today **61**(5), 44–50 (2008).
4. H. Raether, *Surface Plasmons on Smooth and Rough Surfaces and on Gratings*. 1988, Berlin: Springer.
5. F. López-Tejeira, F. J. García-Vidal, and L. Martín-Moreno, "Scattering of surface plasmons by one-dimensional periodic nanoindented surfaces," Phys. Rev. B **72**(16), 161405 (2005).
6. F. López-Tejeira, S. G. Rodrigo, L. Martín-Moreno, F. J. García-Vidal, E. Devaux, T. W. Ebbesen, J. R. Krenn, I. P. Radko, S. I. Bozhevolnyi, M. U. González, J. C. Weeber, and A. Dereux, "Efficient unidirectional nanoslit couplers for surface plasmons," Nat. Phys. **3**(5), 324–328 (2007).
7. J. A. Sánchez-Gil, and A. A. Maradudin, "Surface-plasmon polariton scattering from a finite array of nanogrooves/ridges: Efficient mirrors," Appl. Phys. Lett. **86**(25), 251106 (2005).
8. F. J. García-Vidal, H. J. Lezec, T. W. Ebbesen, and L. Martín-Moreno, "Multiple paths to enhance optical transmission through a single subwavelength slit," Phys. Rev. Lett. **90**(21), 213901 (2003).
9. P. Lalanne, J. P. Hugonin, and J. C. Rodier, "Theory of surface plasmon generation at nanoslit apertures," Phys. Rev. Lett. **95**(26), 263902 (2005).
10. P. Lalanne, J. P. Hugonin, and J. C. Rodier, "Approximate model for surface-plasmon generation at slit apertures," J. Opt. Soc. Am. A **23**(7), 1608–1615 (2006).
11. H. W. Kihm, K. G. Lee, D. S. Kim, J. H. Kang, and Q.-H. Park, "Control of surface plasmon generation efficiency by slit-width tuning," Appl. Phys. Lett. **92**(5), 051115 (2008).
12. A. A. Maradudin, R. F. Wallis, and G. I. Stegeman, "Surface polariton reflection and transmission at a barrier," Solid State Commun. **46**(6), 481–485 (1983).
13. J. Seidel, S. Grafström, L. Eng, and L. Bischoff, "Surface plasmon transmission across narrow grooves in thin silver films," Appl. Phys. Lett. **82**(9), 1368–1370 (2003).

#115245 - $15.00 USD Received 4 Aug 2009; revised 13 Sep 2009; accepted 14 Sep 2009; published 21 Sep 2009

14. J. A. Sánchez-Gil, and A. A. Maradudin, "Near-field and far-field scattering of surface plasmon polaritons by one-dimensional surface defects," Phys. Rev. B **60**(11), 8359–8367 (1999).
15. A. Y. Nikitin, F. Lopez-Tejeira, and L. Martin-Moreno, "Scattering of surface plasmon polaritons by one-dimensional inhomogeneities," Phys. Rev. B **75**(3), 035129 (2007).
16. M. Kuttge, F. J. García de Abajo, and A. Polman, "How grooves reflect and confine surfaceplasmon polaritons," Opt. Express **17**(12), 10385–10392 (2009).
17. G. Veronis, and S. Fan, *Overview of Simulation Techniques for Plasmonic Devices*, in *Surface Plasmon Nanophotonics*, M.L. Brongersma and P.G. Kik, Editors. 2007, Springer. p. 169.
18. R. Gordon, "Light in a subwavelength slit in a metal: Propagation and reflection," Phys. Rev. B **73**(15), 153405 (2006).
19. Snyder, A.W. and J.D. Love, *Optical Waveguide Theory.*
20. B. Sturman, E. Podivilov, and M. Gorkunov, "Eigenmodes for metal-dielectric light-transmitting nanostructures," Phys. Rev. B **76**(12), 125104–125111 (2007).
21. S. E. Kocabaş, G. Veronis, D. A. B. Miller, and S. Fan, "Modal analysis and coupling in metal-insulator-metal waveguides," Phys. Rev. B **79**(3), 035120 (2009).
22. E. N. Economou, "Surface Plasmons in Thin Films," Phys. Rev. **182**(2), 539–554 (1969).
23. J. A. Dionne, L. A. Sweatlock, and H. A. Atwater, "Plasmon slot waveguides: Towards chip-scale propagation with subwavelength-scale localization," Phys. Rev. B **73**(3), 035407–035409 (2006).
24. J. B. Pendry, "Negative refraction makes a perfect lens," Phys. Rev. Lett. **85**(18), 3966–3969 (2000).
25. E. Anemogiannis, E. N. Glytsis, and T. K. Gaylord, "Determination of guided and leaky modes in lossless and lossyplanar multilayer optical waveguides: reflection pole method andwavevector density method," J. Lightwave Technol. **17**(5), 929–941 (1999).
26. S. Fan, "Sharp asymmetric line shapes in side-coupled waveguide-cavity systems," Appl. Phys. Lett. **80**(6), 908–910 (2002).
27. B. Sturman, E. Podivilov, and M. Gorkunov, "Theory of extraordinary light transmission through arrays of subwavelength slits," Phys. Rev. B **77**(7), 075106–075112 (2008).
28. A. D. Rakic, A. B. Djurisic, J. M. Elazar, and M. L. Majewski, "Optical properties of metallic films for vertical-cavity optoelectronic devices," Appl. Opt. **37**(22), 5271–5283 (1998).
29. J. D. Jackson, *Classical Electrodynamics*. 1999: Wiley.

1. Introduction

The realization that structured metallic surfaces can be utilized to realize nanoscale photonic circuitry has opened up a wide range of opportunities for new fundamental research and technological developments [1–3]. A key building block in such circuits is a groove in a metallic film. Individual and periodic arrays of grooves have been used to launch surface plasmon-polaritons (SPPs) from free space optical beams and to generate mirrors, filters, optical cavities, and systems exhibiting light localization [4–16]. These applications all involve a number of fundamental interactions (generation, reflection, and/or transmission) of SPPs with grooves. To better understand the role of SPPs in complex multi-groove structures and to optimize devices based on these geometries, it is important to first understand the interaction of SPPs with a single groove.

We start our study with an investigation of SPP transmission across and reflection from rectangular grooves of varying dimension using full-field electromagnetic simulations based on the 2-dimensional Finite-Difference-Frequency-Domain (FDFD) technique [17]. We then explain the SPP transmission and reflection using an intuitive side-coupled cavity model. The model treats the groove as a truncated metal-dielectric-metal (MDM) SPP waveguide that serves as a side-coupled cavity. The coupling between SPPs on the metal surface and MDM SPPs within the groove is described by a set of complex scattering coefficients, similar to the work by Lalanne et al. on SPP generation at slit apertures [10]. The reflection of MDM SPPs from the bottom of the groove is quantified by a complex reflection coefficient. All of these coefficients were determined for a range of groove widths using numerical simulations. The groove response predicted by the side-coupled cavity model shows excellent agreement with full-field simulations over a wide range of groove dimensions, validating this intuitive model.

The work complements various analytical techniques and simulation approaches that have been utilized to approximate or fully quantify the interaction of SPPs with metallic slits and grooves [9,18]; in our work we provide a quantitative validation of the side-coupled cavity picture that was also suggested by Kuttge et al. earlier this year [16]. For our plasmonic system we directly link the transmission minima with MDM SPP resonances inside the

#115245 - $15.00 USD Received 4 Aug 2009; revised 13 Sep 2009; accepted 14 Sep 2009; published 21 Sep 2009

groove and show how minima result from the destructive interference between directly transmitted SPPs and forward scattered SPPs reemerging from the groove. Our analysis also brings to light the unique role of the magnetic field anti-symmetric MDM SPPs. For sufficiently narrow grooves, this mode is below propagating cutoff and it is evanescent and reactive in nature. For this reason, one might expect it to rapidly decay and be of no consequence in our analysis. Interestingly we find that it can be resonantly enhanced on reflection and give rise to strong groove resonances in the low-loss limit.

2. Calculating SPP transmission, reflection and scattering

We start by describing the results from 2-D FDFD simulations of SPP transmission across a rectangular groove at normal incidence. The simulation boundaries were taken to be perfectly matched layers, and the incident SPP was directionally sourced with a two-layer dipole array using the total field scattered field method and the well-known mode profile for a single interface SPP [4,17]. In this analysis, we use an idealized, lossless metal with $\varepsilon_m = -10$ and a dielectric of $\varepsilon_d = 1$.

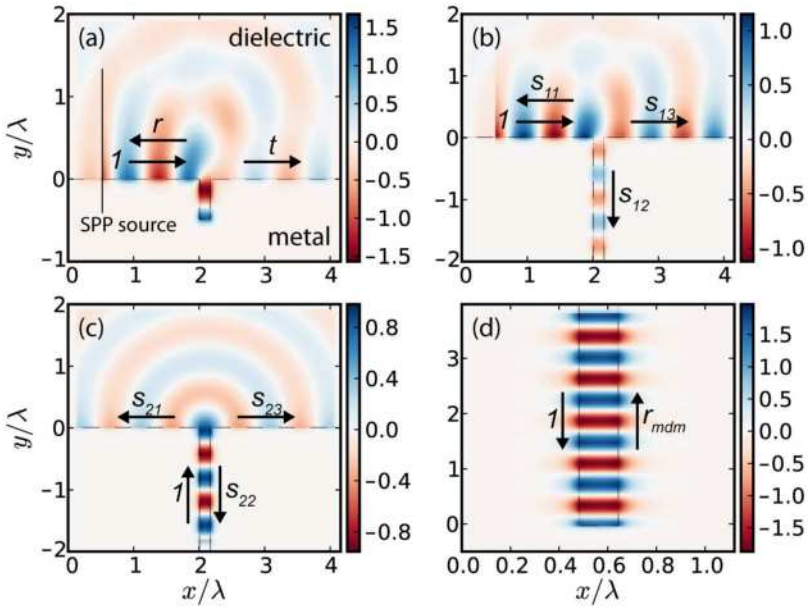

Fig. 1. Full-field electromagnetic simulation of SPPs on metallic grooves and slits. The real value of the magnetic field, H_z, is plotted. $\varepsilon_{metal} = -10$ and $\varepsilon_d = 1$. The groove and slits are all 0.16λ wide, where λ is the free space wavelength. The metal-dielectric interface is demarcated by the black dashed lines. (a) shows a SPP incident on a groove from the left. The depth is 0.48λ. (b) and (c) show a single interface SPP and a MDM SPP, respectively, incident on the mouth of a slit and are used to calculate scattering coefficients at the mouth of the groove. (d) shows a MDM SPP reflecting from the bottom of a groove, which is used to calculate a reflection coefficient. The incident SPPs have a H_z amplitude of unity along the metal-dielectric interface.

Figure 1(a) shows a FDFD simulation for the *H*-field of a SPP incident on a groove. The amplitude of its *H*-field at the metal-dielectric interface was taken to be unity. The groove is near resonance for the incident wavelength, resulting in some SPP back-reflection (22%), significant scattering into free space modes (50%), and a reduced SPP transmission (28%). The power and phase of the transmitted SPP is found by projecting the simulated fields past the groove onto the SPP mode profile. Waveguide theory shows that for a translationally invariant structure reciprocity leads to the orthogonality relation in the numerator of Eq. (1)

#115245 - $15.00 USD Received 4 Aug 2009; revised 13 Sep 2009; accepted 14 Sep 2009; published 21 Sep 2009

[19] (valid for lossy materials as well). This allows us to project the total field (away from the groove) onto any eigenmode as:

$$c_{mode} = \frac{\frac{1}{2}\int_S \left(\vec{E}_{total} \times \vec{H}_{mode} + \vec{E}_{mode} \times \vec{H}_{total}\right) \cdot d\vec{A}}{\int_S \vec{E}_{mode} \times \vec{H}_{mode} \cdot d\vec{A}}, \quad \vec{E}_{total} = \sum_{modes} c_{mode} \vec{E}_{mode} \qquad (1)$$

where E_{total} and H_{total} are the total electric and magnetic fields taken from the simulations, and c_{mode} is the coefficient representing the portion of the total fields in a given mode specified by fields E_{mode} and H_{mode}. S is taken as a plane normal to the metal film and the SPP propagation direction [9]. For the bound and highly confined SPP modes, the finite area of our simulation is sufficient for accurately evaluating these integrals. The dispersion relation and fields for the single interface SPPs are detailed in Raether [4]. Figures 2(a) and 2(c) show the transmitted and reflected SPP power calculated from simulations on grooves of varying dimension using Eq. (1). Overall there are broad regions of high SPP transmission punctuated by sharp transmission minima at narrow groove widths which then broaden at larger widths. The minima occur periodically with increasing depth, and high fields within the groove are observed at all of these minima along with corresponding reflection maxima.

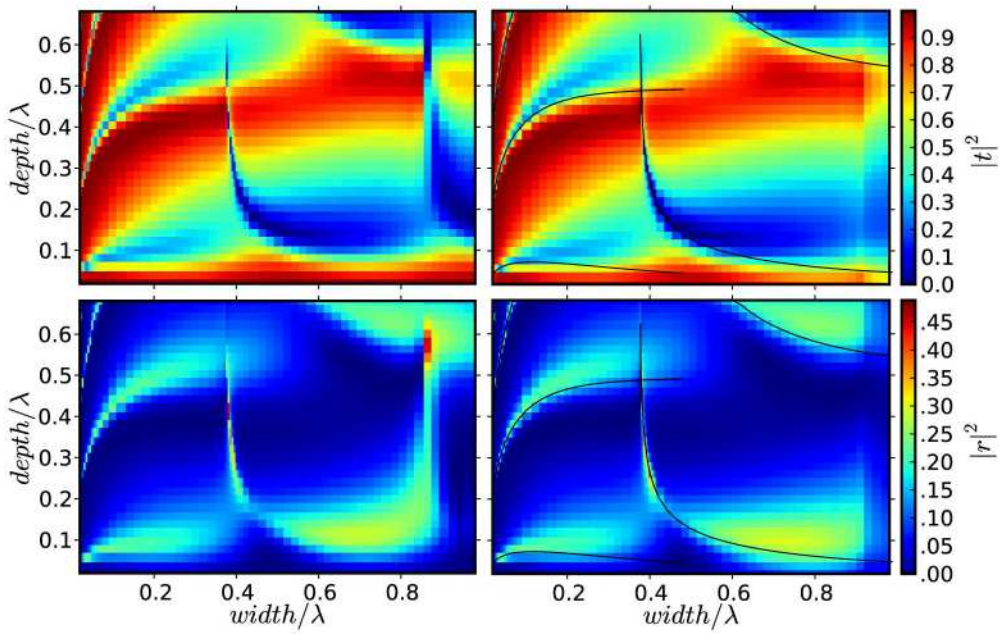

Fig. 2. SPP power transmitted across and reflected from single grooves of different depth and width. (a) and (c) The transmission and reflection, respectively, are calculated from full field 2D FDFD simulations using Eq. (1). (b) and (d) Transmission and reflection, respectively, are calculated from the side-coupled MDM SPP cavity model. The black lines indicate the location of predicted MDM SPP resonances within the groove. Strong transmission minima are observed to be caused by MDM SPP resonances within the groove.

3. Side-coupled cavity model

Below we continue by developing a side-coupled MDM cavity model to explain the presence of the transmission minima and their dependence on the groove parameters. To this end we break-up the interaction of an incident SPP with a groove into its basic processes. An incident SPP can directly be transmitted across a groove or couple sideways to the MDM SPP modes within the groove. The groove itself can serve as a plasmonic cavity in which the MDM SPPs may build up a high energy density after multiple reflections from the mouth and bottom of

#115245 - $15.00 USD Received 4 Aug 2009; revised 13 Sep 2009; accepted 14 Sep 2009; published 21 Sep 2009

the groove. At the mouth of the groove, a fraction of the MDM SPPs will scatter back out into single-interface SPPs. The SPPs that couple in the forward direction will then interfere with the SPPs that are directly transmitted across the groove. According to this line of thinking, dips in the SPP transmission can occur when the SPPs that reemerge from the cavity pickup a substantial amount of phase in the cavity (near π) and destructively interfere with the directly transmitted SPPs. The conditions for this to occur depend on the groove depth, the wavevector of the MDM SPP, and the reflection from the groove terminations. To analyze this in more detail, we first need to quantify the basic scattering processes (scattering into the groove, reflection from terminations, and scattering out of the groove) in terms of a set of complex coefficients.

Figures 1(b)-(d) show simulations of the basic scattering processes that govern SPP transmission across the groove shown in Fig. 1(a). Figure 1(b) shows the interaction of a single interface SPP from the left with a metal slit (i.e. an infinitely deep groove). The scattering coefficients, s_{ij}, describe the coupling from an incident mode i into an outgoing mode j. Here, we will use the index "1" to refer to a single interface SPP on the left side of the groove, "2" to refer to a MDM SPP, and "3" to refer to the SPP on the right side of the groove. Figure 1(c) shows a simulation of the MDM SPP incident on the mouth of a slit. Figure 1(d) shows a simulation of an SPP reflecting from a metal terminated MDM SPP waveguide (i.e. the bottom of a groove). The reflection process is characterized by a complex reflection coefficient r_{mdm}. In addition, both H-field symmetric and anti-symmetric MDM SPP modes exist within the groove and their coefficients will be distinguished by a "+" and "–" respectively. These scattering and reflection coefficients are calculated from the simulated total fields using Eq. (1) with the outgoing SPP and MDM SPP mode profiles. The scattering coefficients between SPPs and MDM SPPs are all normalized by the time averaged magnitude of the incident power. The square of the scattering coefficients represents a fractional coupled power between propagating modes. Following convention, all the reflection and scattering coefficient phases are specified by the E component in the dielectric perpendicular to the axis of translational invariance at the boundaries of the groove.

By considering these basic scattering processes, we can now construct our proposed side-coupled MDM cavity model to predict the steady state transmission and reflection amplitudes:

$$t = s_{13} + \sum_j \frac{s_{1(2j)} s_{(2j)3} r_{mdm,j} e^{i\beta_{mdm,j} 2d}}{1 - r_{mdm,j} s_{(2j)(2j)} e^{i\beta_{mdm,j} 2d}}, \quad r = s_{11} + \sum_j \frac{s_{1(2j)} s_{(2j)1} r_{mdm,j} e^{i\beta_{mdm,j} 2d}}{1 - r_{mdm,j} s_{(2j)(2j)} e^{i\beta_{mdm,j} 2d}} \qquad (2)$$

where β_{mdm} is the propagation constant of the MDM SPP modes and j is either + or - referring to the H-field symmetric and anti-symmetric MDM SPP modes respectively. In the derivation of these equations, we use the fact that symmetric and anti-symmetric MDM SPP modes cannot scatter into each other at a boundary with mirror symmetry. The predicted transmission and reflection intensities, $|t|^2$ and $|r|^2$, according to this model are plotted in Fig. 2(b) and 2(d) for comparison to the projected transmission and reflection from full-field simulations. The super-imposed black lines show the locations of MDM SPP groove cavity resonances determined as the depths that minimize the denominators of Eq. (2) at each width. The good agreement between the side-coupled MDM SPP cavity model and the FDFD simulations validates our model and shows that the sharp transmission minima are caused by destructive interference between the directly transmitted SPPs and the forward scattered SPPs emerging from groove. Figure 3(a) and 3(b) display detailed agreement between the transmission amplitude and phase as calculated from the full-field simulations and Eq. (2) (the time dependence of phase is taken as $e^{-i\omega t}$). This further lends credibility to our model.

#115245 - $15.00 USD Received 4 Aug 2009; revised 13 Sep 2009; accepted 14 Sep 2009; published 21 Sep 2009

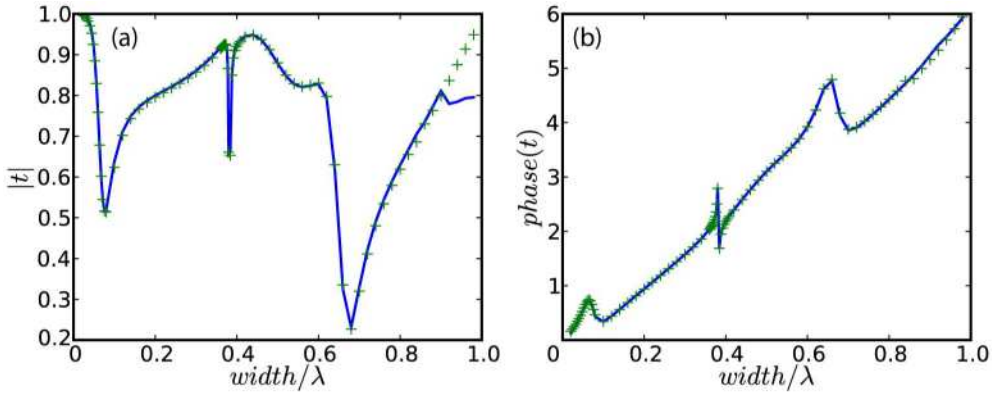

Fig. 3. Transmission amplitude (a) and phase (b) for square grooves (depth equal to width) of varying dimension. Transmission calculations from the FDFD simulation (+ green) show excellent agreement with the side-coupled MDM cavity model predictions (- blue).

3.1 Assumptions and limitations of the side-coupled cavity model

Two approximations were used in the derivation of Eq. (2). In a MDM modal expansion there are an infinite number of higher order metal clad waveguide modes within the groove, but for sufficiently narrow grooves they have complex propagation constants that correspond to rapidly decaying waves [20, 21]. For this reason, they should not scatter back out of a groove with significant depth and can be neglected. The other assumption we make is that the single interface SPP scatters into or out of MDM modes at the top of the groove and not the bottom. This is accurate for sufficiently deep grooves as the SPP field decays quickly inside the metal. These assumptions break down though in the wide and shallow groove limits as evidenced by the discrepancies in this regime in Figs. 2(a)-(d). In particular the first TM metal clad waveguide mode exhibits cutoff at a groove width of 0.9λ (Eq. (3)), and the side-coupled MDM SPP cavity model fails to accurately predict the FDFD results for widths greater than 0.85λ. The penetration depth of the SPP in the metal is 0.05λ so the model also fails to accurately predict FDFD results for depths less than approximately 0.1λ. Aside from these regions the side-coupled MDM SPP cavity model shows excellent agreement with the full-field simulation. Identical levels of agreement are seen when comparing transmission and reflection phase between the FDFD simulation and the side-coupled MDM SPP cavity model (not shown here).

4. Model components: width dependence of MDM SPPs and scattering coefficients

After having established the validity of the side-coupled cavity model, it is of value to have a closer look at the dependence of the scattering coefficients on the groove dimensions. A deeper understanding of these dependencies will also provide a better insight into the transmission and reflection behavior shown in Fig. 2. The dependence of the parameters on groove width is of particular interest as the width governs the number and type of modes that are supported by an MDM waveguide. To determine the number and nature of the modes that are allowed at each width, we start with a brief look at the dispersion relationship for MDM modes. Figures 4(a) and 4(b) show the width-dependence of the real and imaginary part of the propagation constant, β_{mdm}, for the *H*-field symmetric and anti-symmetric SPP modes supported by an MDM waveguide. The value of β_{mdm} is normalized by the magnitude of the vacuum wave vector. These plots are calculated from the dispersion relationship for transverse magnetic modes (TM):

$$\tan\left(k_{\perp d}w\right)+2i\left(k_{\perp d}k_{\perp m}\Big/\varepsilon_d\varepsilon_m\right)\Big/\left(k_{\perp d}{}^2\Big/\varepsilon_d{}^2+k_{\perp m}{}^2\Big/\varepsilon_m{}^2\right)=0,\quad k_\perp=\sqrt{\varepsilon-\beta_{mdm}^2}\qquad(3)$$

#115245 - $15.00 USD Received 4 Aug 2009; revised 13 Sep 2009; accepted 14 Sep 2009; published 21 Sep 2009

Here, ε is the permittivity of either the dielectric or the metal, w is the width of the dielectric layer normalized to the wavelength. $k_{\perp}$ is the magnitude of the wave vector component normal to the MDM interfaces. The equation is equivalent to the separate symmetric and anti-symmetric forms used by other authors describing the MDM SPP eigenmodes in greater detail [22,23]. The symmetric MDM SPP is propagating for all widths with real-valued β_{mdm} in our lossless case. The *H*-field anti-symmetric MDM SPP has a cutoff width where it transitions from propagating to evanescent. The evanescent, anti-symmetric MDM SPP is reactive in nature with an imaginary β_{mdm} closer to cutoff and a complex β_{mdm} at even narrower widths (not shown). It carries no time-averaged power in the lossless limit.

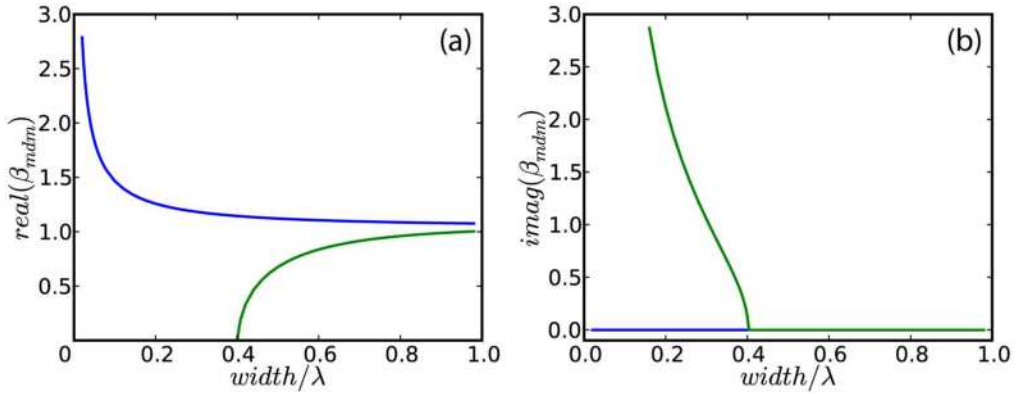

Fig. 4. Plots of the real (a) and imaginary (b) parts of the propagation constant for symmetric (blue) and anti-symmetric (green) MDM SPP modes. $\varepsilon_m = -10$ and $\varepsilon_d = 1$. β_{mdm} is normalized to the magnitude of the vacuum wavevector.

Figure 5(a) and 5(b) shows the relevant scattering coefficients as a function of the MDM waveguide width. They capture the coupling between the various modes that follow from the dispersion relation above. The behavior of these coefficients has several characteristics that are worth noting. Reciprocity dictates that the coefficients describing how a single interface SPP incident from the left couples to a symmetric (s_{12+}) or anti-symmetric (s_{12-}) MDM SPP mode are identical to the coefficients describing the reverse processes, s_{2+1} and s_{2-1}, respectively [19]. The scattering coefficients describing the coupling between the MDM modes and the SPP on the right of the groove are identical to those describing the coupling to SPPs on the left side with one notable exception: the *H*-field symmetric MDM SPP excites single interface SPPs on the left and right that are out of phase by π. Generally significant direct SPP transmission across the groove (s_{13}) is seen even at larger widths. In contrast direct reflection is low (s_{11}). The reflection coefficients for MDM SPP modes at the mouth of the groove (s_{22}) is high near cutoff for the anti-symmetric SPP and near zero width for the symmetric SPP due to a large mismatch between β_{mdm} and the free space wavevector magnitude. The observed discontinuities in slope are due to the appearance of the propagating or power carrying anti-symmetric MDM SPP at 0.4λ and the first transverse magnetic (TM) MDM waveguide mode at 0.9λ.

#115245 - $15.00 USD Received 4 Aug 2009; revised 13 Sep 2009; accepted 14 Sep 2009; published 21 Sep 2009

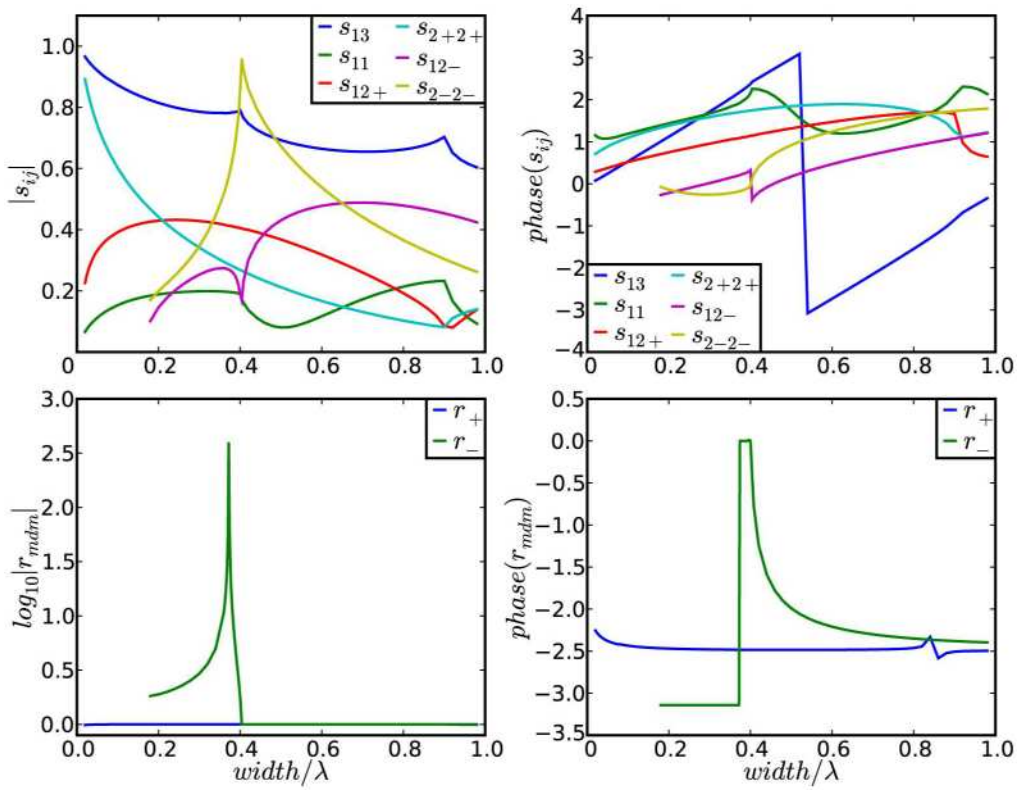

Fig. 5. Scattering and reflection coefficients. (a) and (b) show the amplitude and phase of the scattering coefficients calculated at the mouth of a slit. The first number in the subscript refers to the mode that is scattered from and the second to the mode that is scattered into. 1 and 3 refer to the single interface SPPs on the left and right side respectively. 2+ and 2- refer to the field symmetric and field anti-symmetric MDM surface plasmons respectively. (c) and (d) show the reflection coefficient amplitude and phase as calculated from the bottom of an infinitely deep groove.

Figures 5(c) and 5(d) show the reflection coefficients as calculated with Eq. (1) from simulations as depicted in Fig. 1(d). These coefficients deserve extra attention as they are responsible for several unique features in the SPP groove transmission and reflection plots of Fig. 2. As expected for a lossless metal, all the propagating MDM SPPs exhibit unity reflection. The metal bottom tends to expel the parallel E-field so the reflection phase is close to π for propagating modes. For metals with a finite conductivity the resulting field penetration results in somewhat greater reflection phases. The evanescent, field anti-symmetric MDM SPP excites a single interface SPP mode along the metal end-face of the MDM and is resonantly enhanced upon reflection. The reflection peak corresponds to an optimal excitation of the single interface SPP mode along the metal end face of groove, and a π phase transition is observed at this width. For evanescent, reactive modes energy conservation constrains the phase not the amplitude so there is no violation as in other cases presented in 1-dimensional systems [24, 25]. In particular for the lossless case, the reflection phase for a reactive mode can only be 0 or π, which our calculations are consistent with.

5. Analysis and interpretation

Using our enhanced knowledge of the dependence of the scattering and reflection coefficients on the MDM width, we are now in a position to provide a more detailed analysis of the observed features in Fig. 2. As discussed previously, the transmission minima here originate from the destructive interference between directly transmitted SPPs and SPPs that scatter out

#115245 - $15.00 USD Received 4 Aug 2009; revised 13 Sep 2009; accepted 14 Sep 2009; published 21 Sep 2009

of the groove at resonance. The MDM SPP resonances that occur for the evanescent, reactive MDM SPP modes are different in nature than the resonances arising from the propagating MDM SPPs. Propagating MDM SPPs resonate whenever there is an integer 2π round trip phase within the groove, but the round trip amplitude decrease is always greater than zero due to scattering losses and this limits the intensity of the resonance. Conversely, reactive MDM SPP resonances occur at depths where the round trip amplitude decrease is zero, but the round trip phase is never exactly 2π due to losses and this limits the intensity of reactive resonances.

Propagating resonances arise for both the field symmetric MDM SPP at widths below 0.4λ and the field anti-symmetric MDM SPP mode at widths between 0.4 and 0.85λ (Fig. 4(a)). These resonances occur periodically with depth every time the groove cavity round trip phase is an integer multiple of 2π. This results in several blue bands of transmission minima at different depths. The exact resonant depth is critically dependent on the propagation constant of the MDM SPPs, real$\{\beta_{mdm}\}$, and the reflection phase at the terminations of the groove, s_{22} and r_{mdm}. For the symmetric MDM SPP, the sharp increase of real$\{\beta_{mdm}\}$ at small widths leads to a quick drop in the resonant depth needed to achieve an integer 2π round trip phase. Similarly, the rapid increase of real$\{\beta_{mdm}\}$ for the anti-symmetric MDM SPP starting at 0.4λ leads to a drop in resonant depth with increasing widths. The shift in resonant depth due to reflection phase is less significant than that due to β_{mdm} because the reflection phases are relatively constant for the symmetric MDM SPP and roughly cancel for the anti-symmetric MDM SPP.

The intensity of the resonance is limited by scattering loss which results in a reflection amplitude of less than unity at the mouth of the groove, s_{22}. s_{22} is highest for the symmetric and anti-symmetric MDM SPPs near 0λ and 0.4λ respectively. The strong reflections here give rise to higher quality factor (Q) resonances and sharper transmission minima. As we move to larger groove widths, the reflection of MDM SPPs (s_{22}) decreases and the resonances and corresponding transmission minima broaden.

In addition, the transmission minima do not always coincide exactly with the groove resonances. At narrow widths, direct SPP transmission across the groove is close to unity so that scattering from the MDM SPP resonance can only interfere destructively to produce transmission minima (energy conservation). This results in transmission minima that coincide with the peak MDM SPP resonance. However, at larger widths direct SPP transmission across the groove decreases, and scattering from the MDM SPP resonance can interfere both constructively to produce transmission maxima as well as destructively to produce minima. This produces a distinct Fano lineshape with transmission minima and maxima located on opposing sides of the MDM SPP resonance as seen in Fig. 2(b). This effect is very similar to that in the first side-coupled cavity paper showing Fano interference by S. Fan [26].

Lastly, the resonance for widths between 0.374λ and 0.4λ is caused by the reactive anti-symmetric MDM SPP (Fig. 4(b)). Despite the decay of this mode, the amplified reflection from the bottom of the groove (r_{mdm}) can result in a strong resonance. This resonance is not allowed though for widths smaller than 0.374λ because the π phase on reflection from the metal produces roundtrip destructive interference. Past its peak though, r_{mdm} goes through a π phase transition producing resonance within the groove. The exact depth of this resonance is determined by the decay of the MDM SPP and the amplification from the quickly varying metal reflection. A simulation of one groove displaying this resonance is shown in Fig. 6.

#115245 - $15.00 USD Received 4 Aug 2009; revised 13 Sep 2009; accepted 14 Sep 2009; published 21 Sep 2009

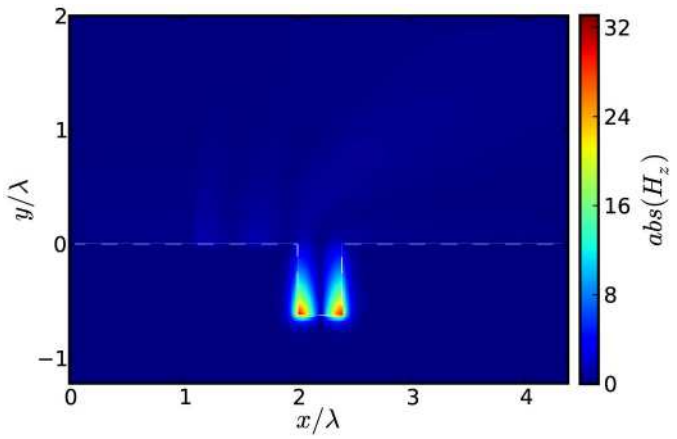

Fig. 6. FDFD simulation of a SPP incident on a groove in a metallic film. The SPP is incident from the left and the absolute value of the magnetic field, abs(H_z), is plotted for the case that $\varepsilon_{metal} = -10$, and $\varepsilon_i = 1$. The metal-dielectric interface is demarcated by the white dashed lines, and the incident SPP has a field of unity there. The groove is 0.374λ wide and 0.62λ deep. A resonance is observed within the groove arising from the *H*-field anti-symmetric, reactive MDM mode and causes destructive interference with minimum transmission.

6. Concluding remarks

Many calculations of SPPs and waveguide modes in MDM and hole structures only include the propagating solutions that constantly carry power in the forward direction. Other papers have shown that the full spectrum of MDM modes are needed for a complete analytical description of scattering at the boundary of MDM structures [20, 21]. The propagation of reactive modes between interfaces has also been shown to provide a correction when calculating extraordinary transmission through an array of slits [27]. In short cavities, reactive modes can be expected to offer significant corrections; however, with long structures the greater attenuation of the reactive modes frequently makes them less important than the propagating modes. In a metallic groove though, reactive modes can be resonantly enhanced (reflection greater than one) upon reflection from the bottom metal boundary. As a result, reactive SPP modes can dominate the response of a groove, cause sharp transmission resonances, and produce high field intensities, even at depths where significant attenuation is expected. There is the potential to engineer grooves using reactive SP modes to achieve high field amplification for use with detectors or light emitters.

For real metals exhibiting material loss, the MDM SPP groove resonances are dampened, but qualitatively similar behavior is observed. Figure 7(a) and 7(b) show simulated and modeled SPP groove transmission for Ag at λ = 875nm, using a complex dielectric constant of $\varepsilon_{Ag} = -30.240 + 2.217i$ [28]. With material losses the reactive MDM SPP resonance is dampened significantly, but its effects can still be observed close to cutoff. Gain media could potentially counter the loss and utilize these reactive MDM SPP modes for SPP modulation and switching.

#115245 - $15.00 USD Received 4 Aug 2009; revised 13 Sep 2009; accepted 14 Sep 2009; published 21 Sep 2009

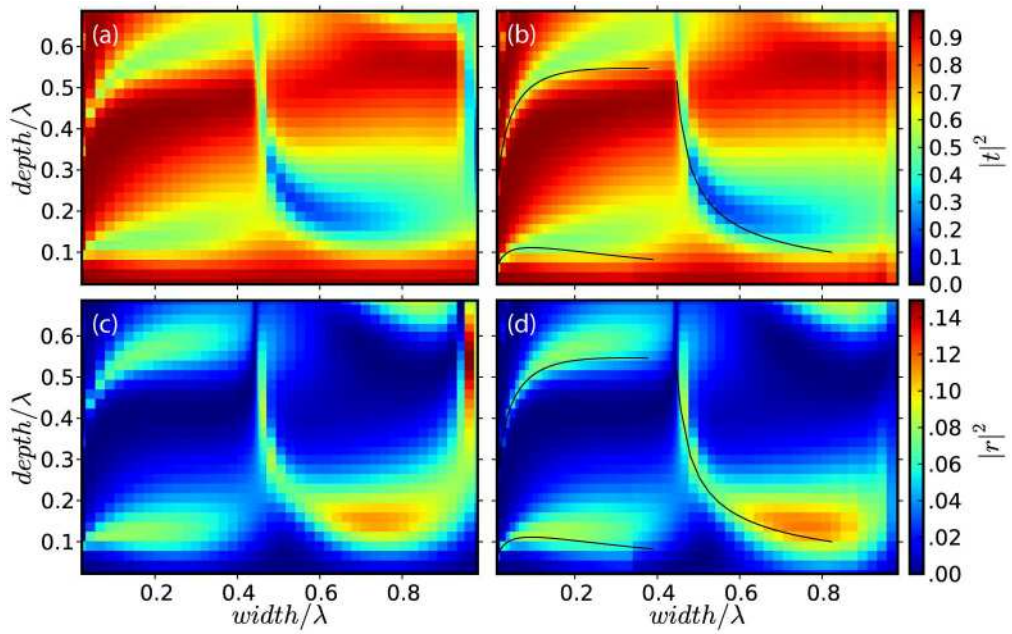

Fig. 7. Transmitted and reflected SPP power across single grooves of varying dimension for Ag at λ = 875nm. ε_{Ag} = 30.240 + 2.217i. (a) and (c) are full field simulations. (b) and (d) are calculations from the side-coupled MDM SPP cavity model. The black lines represent model calculated MDM SPP resonances. These resonances are dampened by loss, but the same general features and trends are still observable.

In conclusion, using a numerical study of scattering and reflection coefficients calculated from FDFD simulations we have shown that the width and depth dependent SPP transmission across a groove can be accurately predicted by an intuitive side-coupled MDM SPP cavity model over a large range of groove dimensions. Transmission minima are shown to be caused by cavity resonances of the propagating and reactive MDM SPPs. Reactive SPPs were shown to be significantly amplified on reflection from a metal boundary leading to strong resonances, sharp transmission minima and high field intensities within the groove.

Appendix: Power conservation and reflection of reactive modes

We can obtain some general understanding of reactive modes by considering plane wave modes. Although a lossless, lone reactive mode carries no net power, a superposition of forward and backward reactive modes can carry net power. Calculating the complex power of a plane wave and its reflection we obtain the results of Eq. (4) below.

$$\begin{aligned} &H_z = \left(e^{ik_\perp x} - re^{-ik_\perp x}\right)e^{ik_\parallel y}; \quad E_y = \tfrac{k_\perp}{\varepsilon}\left(e^{ik_\perp x} + re^{-ik_\perp x}\right)e^{ik_\parallel y}; \quad r = r' + ir''; \quad r', r'' \in \mathbb{R} \\ &S_x = \tfrac{1}{2}E_y H_z^* = \tfrac{-ik_\perp e^{-2k_\parallel y}}{\varepsilon}\left[\tfrac{i}{2}e^{-2k_\perp r'' x} - \tfrac{i}{2}|r|^2 e^{2k_\perp r'' x} - r''\cos\left(2k_\perp' x\right) + r'\sin\left(2k_\perp' x\right)\right] \end{aligned} \tag{4}$$

The real part of the complex Poynting vector is net, time-averaged power while the imaginary part represents reactive, oscillatory power whose time-averaged contribution is zero [29]. Energy conservation requires that $real(S_x) \geq 0$ as we cannot reflect more power than we send in. For propagating modes $k_\perp$ is real and energy conservation gives the amplitude constraint that $|r|^2 \leq 1$. For reactive plane waves $k_\perp$ is imaginary so the imaginary part of the reflection coefficient results in time-averaged power flow. Thus energy conservation for a reactive wave results in a phase constraint requiring that $imag(r) \leq 0$. For a reactive wave ending on a lossless metal no power is lost to absorption so the reflection phase can only be 0 or π.

#115245 - $15.00 USD Received 4 Aug 2009; revised 13 Sep 2009; accepted 14 Sep 2009; published 21 Sep 2009

Even though reactive modes attenuate significantly with distance, they can be amplified significantly upon transmission or reflection at a metal dielectric interface as energy conservation now constrains the phase and not the amplitude. The reflection of a plane wave at a single interface is expressed by Fresnel's equation in terms of surface impedances in Eq. (5).

$$r = \frac{Z_m - Z_d}{Z_m + Z_d}, \quad Z_m = {k_{\perp m}}/{\varepsilon_m}, \quad Z_d = {k_{\perp d}}/{\varepsilon_d}, \quad k_{\perp d} = \sqrt{\varepsilon_d - k_{\parallel}^2} \tag{5}$$

where $k_{\perp}$ is the wavevector component perpendicular to the interface and $k_{\parallel}$ is the wavevector component parallel to the interface. The high impedance mismatch of reactive waves at a metal-dielectric interface results in amplified reflection and transmission at the interface. This forms the basis for the well-known near-field imaging or perfect lensing with negative permittivity materials [24]. In imaging with a perfect lens, a flat response function is desired, which can be attained when $\varepsilon_m = -\varepsilon_d$ at the surface plasmon frequency. For $\varepsilon_m > -\varepsilon_d$ the SPP resonance is accessible at lower wavevectors leading to a resonant reflection peak and a π phase transition corresponding to the excitation of the single interface surface plasmon. At the surface plasmon resonance excitation of the SPP leads to significant losses in the metal and power transfer is maximized with a reflection phase of $-\pi/2$.

Acknowledgments

The authors would like to thank Ragip Pala and Edward Barnard for helpful discussions. This work was funded by the Department of Energy (Grant No. F49550-04-10437).

#115245 - $15.00 USD Received 4 Aug 2009; revised 13 Sep 2009; accepted 14 Sep 2009; published 21 Sep 2009